THE JOURNAL OF PHYSICAL CHEMISTRY A

Article

pubs.acs.org/JPCA

Reaction of Methacrolein with the Hydroxyl Radical in Air: Incorporation of Secondary O_2 Addition into the MACR + OH Master Equation

Gabriel da Silva*

Department of Chemical and Biomolecular Engineering, The University of Melbourne, Victoria 3010, Australia

Supporting Information

ABSTRACT: Methacrolein (MACR) plays an important role in atmospheric chemistry within the planetary boundary layer, as it is one of the major oxidation products of isoprene and has a short lifetime toward the hydroxyl radical (OH). In this study, quantum chemical techniques and statistical reaction rate theory have been used to simulate the addition of OH to MACR at conditions representative of the troposphere. In this chemically activated reaction, the time scales for product formation versus collisional deactivation of the vibrationally excited adduct are explicitly considered. Furthermore, the subsequent addition of O_2 is also incorporated within a single master equation, so as to investigate doubly activated peroxyl radical formation. The major reaction product of OH addition to MACR is the $HOCH_2C^{\bullet}(CH_3)CHO$ radical formed via addition to the outer (β) carbon. This radical is predominantly in the *Z* isomer although around a third of the population is quenched as the higher-energy *E* isomer. Calculated rate constants agree well with experiment when using M06−2X/aug-cc-pVTZ barrier heights, but are somewhat overpredicted using G3SX energies. The overall rate constant is controlled by competition between dissociation of the MACR···OH van der Waals complex back to reactants and isomerization on to MACR−OH adducts, which takes place on a time scale of several nanoseconds, but collisional deactivation of the MACR−OH adducts occurs on a time scale that is around an order of magnitude longer. When O_2 addition is included in the master equation, we observe that the MACR−OH adducts are removed by reaction with O_2 on a similar time scale to collisional deactivation. Around 50% of the subsequent peroxyl radical population is formed with some identifiable excess vibrational energy above singly activated $[MACR{-}OH{-}O_2]^*$, with around 20% provided with an additional 20 kcal mol^{-1} (>40 kcal mol^{-1} relative to quenched $MACR{-}OH{-}O_2$) that can go into further unimolecular reaction. This double activation process is expected to lead to some prompt unimolecular decomposition of excited $[MACR{-}OH{-}O_2]^{**}$ peroxyl radicals to yield products including hydroxyacetone and methylglyoxal, regenerating the initiating OH radical in the process.

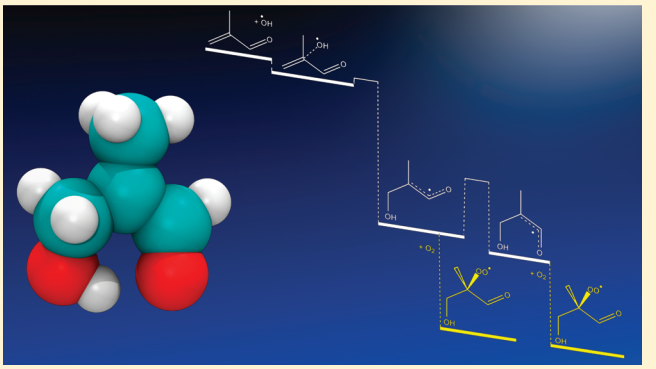

INTRODUCTION

Chemistry in the planetary boundary layer (PBL) of Earth's atmosphere is profoundly influenced by the presence of volatile organic compounds (VOCs) and their oxidation products, OVOCs. The photochemical oxidation of these compounds impacts the oxidative capacity of an air mass and is involved in the production of tropospheric ozone and secondary organic aerosols, impacting air quality and the formation of cloud condensation nuclei and thus cloud cover and albedo. It is emerging that current atmospheric chemistry models cannot reproduce important phenomena within the pristine forested boundary layer when there are high isoprene fluxes as well as low levels of NO_x, which would otherwise facilitate ozone formation and cycling of HO_2 to OH.[1−6]

Biogenic isoprene is the largest VOC emitted to pristine forested regions of the PBL, and the second largest VOC source to the atmosphere overall, behind methane. Unlike methane, however, isoprene is highly reactive toward the hydroxyl radical, with a lifetime of around an hour (vs 5 to 10 years). This allows isoprene to be predominantly removed within the boundary layer, controlling the oxidative capacity and OH reactivity of this region. Methacrolein (MACR) and methyl vinyl ketone (MVK) are the primary oxidation products of isoprene,[7−9] and because they too react rapidly with OH, they can both be formed and removed within the forested boundary layer within a single day. In order to understand and model, for example, oxidative capacity,[4] OH reactivity,[5] and HO_2:OH ratios[6] in the forested boundary layer as an air mass ages across the diurnal cycle we need to have an accurate description of the MACR and MVK sinks, principally their reactions with OH.

Received: April 20, 2012
Revised: May 15, 2012
Published: May 16, 2012

DOI: 10.1021/jp303806w
J. Phys. Chem. A 2012, 116, 5317−5324

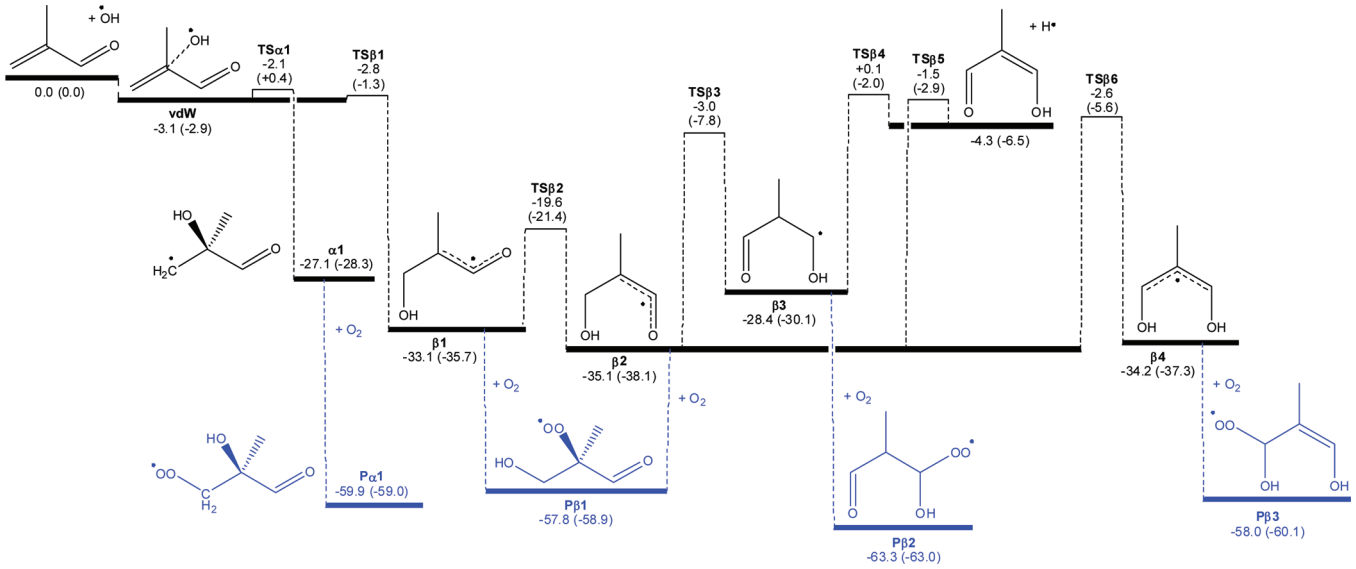

Figure 1. Energy surface for OH addition to MACR. Energies are 0 K enthalpies at the G3SX (M06−2X/aug-cc-pVTZ)) levels of theory.

The initial stages of MACR photooxidation are relatively well-characterized. MACR is predominantly removed through reaction with OH, with lesser amounts of photolysis.[10] The MACR + OH reaction proceeds with $k = 3 \times 10^{-11}$ cm^3 molecule^{-1} s^{-1} at 298 K.[10−13] Around half of the reaction flux involves abstraction (1), with the other half forming the β OH addition product (2), leaving negligible quantities as the α addition product (3). Theoretical studies of the MACR + OH reaction produce results that are generally in agreement with experiment.[14,15]

$$CH_2C(CH_3)CHO + {}^{\bullet}OH \rightarrow CH_2C(CH_3)C^{\bullet}O + H_2O \quad (1)$$

$$CH_2C(CH_3)CHO + {}^{\bullet}OH \rightarrow HOCH_2C^{\bullet}(CH_3)CHO \quad (2)$$

$$CH_2C(CH_3)CHO + {}^{\bullet}OH \rightarrow {}^{\bullet}CH_2C(OH)(CH_3)CHO \quad (3)$$

When considering the photochemical oxidation of MACR, the major uncertainties relate not to the kinetics or products of OH-initiated oxidation, but to the fate of these reaction products. Recently, Asatryan et al.[16] theoretically studied the reactions of the α and β acrolein−OH addition products with O_2, which serve as proxies for the corresponding MACR/MVK + OH products. Because the subsequent peroxyl radicals have reactive β-hydroxyperoxyl[17−19] and α-formylperoxyl[20,21] functionality they were shown to undergo unimolecular dissociation with relatively low barriers, equivalent to around the reactant energies. Furthermore, it was proposed that a double chemically activated reaction, in which the [acrolein−OH]* adduct associates with O_2 before it can be thermalised through bath gas collisions, could lead to prompt peroxyl radical dissociation, in mechanisms that regenerate the initiating hydroxyl radical. A recent experimental study on the OH-initiated oxidation of MACR has provided confirmation of hydroxyacetone production and OH regeneration from unimolecular peroxyl radical decomposition,[22] although the importance of the double activation mechanism remains to be determined.

This study reinvestigates the MACR + OH addition reactions, considering the time scales for chemical reaction and collisional deactivation in this chemically activated process. Further to this, the subsequent addition of O_2 to the reaction products is incorporated into a single master equation (i.e., MACR + OH + O_2), so as to examine competition between collisional deactivation and O_2 addition. This work identifies that double activation via O_2 addition to vibrationally excited [MACR−OH]* radicals is an important process under tropospheric conditions. These peroxyl radicals are expected to achieve prompt hydroxyl radical recycling along with the production of the known isoprene oxidation products hydroxyacetone and methylglyoxal.

METHODS

Electronic Structure Calculations. Stationary points in the MACR + OH + O_2 reaction system were located with the M06−2X and B3LYP DFT methods, using the 6-31G(2df,p) basis set. Frequency calculations were performed on all structures and intrinsic reaction coordinate scans were used to verify transition state connectivity. For the M06−2X structures, a further single-point energy calculation was performed with the large aug-cc-pVTZ basis set to arrive at the final energies reported here. The B3LYP structures were used in subsequent G3SX theory energy calculations. The multilevel G3SX theoretical method combines single-point wave function theory energy calculations increasing in level from HF through QCISD(T) theory with basis sets of incrementally decreasing size, along with an empirical scaling correction, to arrive at accurate molecular energies. Both the G3SX[23] and M06−2X[24] model chemistries are accurate for barrier heights and main group thermochemistry, with mean errors expected to be on the order of 1 and 2 kcal mol^{-1} for the two respective methods.[23−25] All calculations were performed using Gaussian 09.[26] Optimized coordinates, vibrational frequencies, and moments of inertia subsequently used in the master equation modeling are supplied as Supporting Information.

Master Equation Simulations. The Multiwell2011.3 suite of programs was used for all statistical reaction rate simulations.[27−30] Calculations made use of the optimized M06−2X structural properties, with simulations performed

DOI: 10.1021/jp303806w
J. Phys. Chem. A 2012, 116, 5317−5324

using energies from both the M06−2X/aug-cc-pVTZ and G3SX model chemistries.

Densities and sums of states for RRKM theory microcanonical rate constants are from Stein−Rabinovitch−Beyer−Swinehart counts, with an energy grain of 10 cm^{-1} applied over 2999 grains. For use with the continuum master equation, densities and sums of states are evaluated up to 200 000 cm^{-1} over 3001 grains. Statistical mechanics models of wells and transition states make the conventional assumption of a symmetric top with active 1D and inactive 2D external rotors (the *K*-rotor and *J*-rotor, respectively). Corrections are applied for symmetry, optical isomerism, and electronic degeneracy as appropriate. Quantum mechanical tunnelling is incorporated for H-shift reactions via unsymmetrical Eckart barriers.

Master equation simulations were performed at 298 K for 1 atm of N_2 (as a proxy for air, which has similar CET properties). All $C_4O_2H_7$ wells are assigned Lennard−Jones parameters σ = 6.0 Å and ε/k_b = 450 K. Energy transfer is treated with the single exponential down model with ΔE_{down} = 200 cm^{-1} for N_2−$C_4O_3H_8$ collisions. It was found that simulations required less than 1000 collisions (equivalent to 74.3 ns) to achieve steady-state product yields and energy distributions. So as to accurately characterize low-yielding channels, each simulation consists of 100 million trials, allowing yields to be reliably determined down to around 0.00001%.

RESULTS AND DISCUSSION

OH Addition Mechanisms. An energy surface for addition of OH to the α and β carbon atoms in MACR is provided as Figure 1. Optimized structures for the $C_4O_2H_7$ wells and transition states are illustrated in Figures 2 and 3. We find that

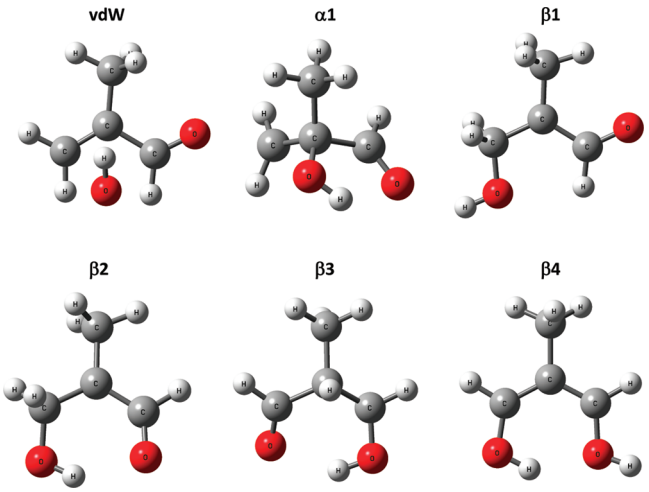

Figure 2. Optimized structures for $C_4O_2H_7$ minima in the MACR + OH α and β addition mechanisms, at the M06−2X/6-31G(2df,p) level of theory.

the two theoretical methods are in relatively good agreement, with a mean unsigned deviation of 2.0 kcal mol^{-1} (the M06−2X energies are systematically below the G3SX ones, with a mean signed deviation of −1.5 kcal mol^{-1}). From Figure 1 we see that reaction proceeds via the initial barrierless formation of a prereaction complex (**vdW**), a weak van der Waals complex that sits at around 3 kcal mol^{-1} below the reactant energies. Note that this structure could not be located at the B3LYP/6-31G(2df,p) level, and the G3SX energy was arrived at by using the corresponding M06−2X structure. For the α mechanism,

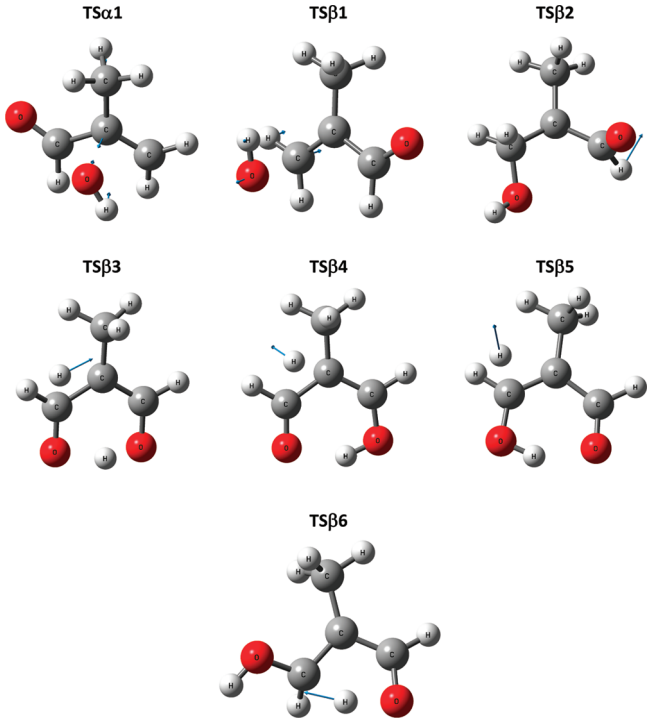

Figure 3. Optimized structures for $C_4O_2H_7$ transition states in the MACR + OH α and β addition mechanisms, at the M06−2X/6-31G(2df,p) level of theory with displacement vectors illustrated for the imaginary mode.

the MACR···OH complex proceeds to form the $^{\bullet}CH_2C(OH)(CH_3)CHO$ radical ***α*1** via a C−OH bond forming transition state that lies at around the entrance channel energy (**TS*α*1**); at the M06−2X/aug-cc-pVTZ level this transition state is just above the reactant energies, whereas the G3SX calculations place it 2.1 kcal mol^{-1} below the reactants. Formation of the MACR−OH adduct is over 25 kcal mol^{-1} exothermic.

For OH addition at the β carbon the transition state for C−OH bond formation (**TS*β*1**), yielding $HOCH_2C^{\bullet}(CH_3)CHO$, is lower in energy at 2.8/1.3 kcal mol^{-1} below the reactants at the G3SX/M06−2X levels. This is consistent with the β addition process dominating over α addition, experimentally. Following formation of the new C−OH bond the [MACR−OH]* adduct is in the *E* isomer (***β*1**), with the formyl and hydroxymethyl substituents on the same side of the C═C double bond. The MACR−OH adduct is formed with around 35 kcal mol^{-1} energy relative to the reactants, where the additional energy compared to the alpha MACR−OH addition product arises from resonance stabilization between $C{=}C{-}O^{\bullet}$ add $C^{\bullet}{-}C{=}O$ (vinoxyl) structures. Isomerization of ***β*1** to ***β*2** by rotation about the C═C double bond (although possessing a C−C resonance structure) requires a barrier of around 15 kcal mol^{-1} (**TS*β*2**) which places it about 20 kcal mol^{-1} below the reactants. The *Z* isomer (***β*2**) is the global minima for $HOCH_2C^{\bullet}(CH_3)CHO$, and this reaction releases a further 2 kcal mol^{-1} of electronic energy out into the active degrees of freedom in the [MACR−OH]* adduct. From here, a number of interesting reaction pathways have been identified proceeding at below the entrance channel energy. The MACR−OH adduct can transfer a hydrogen atom from the hydroxyl moiety to the formyl group, producing an α-hydroxyalkyl radical (***β*3**). This radical can then β-scission a H atom to yield the enol $OCHC(CH_3){=}CHOH$ with barrier

DOI: 10.1021/jp303806w
J. Phys. Chem. A 2012, 116, 5317−5324

at around the entrance channel energy. This species can also be formed directly from **β2** via **TSβ5**, with a slightly lower barrier. Finally, H atom transfer can also occur in **β2** from the β carbon to the formyl oxygen, via **TSβ6**, producing a disubstituted α-hydroxyalkyl radical (**β4**). The barrier for this reaction is slightly greater than that for **TSβ3**, but is still several kcal mol^{-1} below the entrance channel. It is possible to again β-scission a H atom from this radical, yielding the same enol product as **β2** and **β3**, but this proceeds at above the entrance channel energy and is not included in the master equation modeling. Similarly, **β3** could lose an H atom to form a dialdehyde (OCHCH-(CH_3)CHO), but this is again above the entrance channel energy (interestingly, the aldehyde is actually less stable than the enol tautomer because it lacks the additional stabilization arising from conjugation of the C═C and C═O double bonds). These isomerization and β-scission reactions turn out to be of only minor importance in this MACR + OH reaction at room temperature and pressure (vide infra), although similar processes may be of significance in the reactions of other OVOCs. There is a growing interest in the atmospheric chemistry of enols,[31−33] and the reactions identified here may help illuminate some new routes to their formation.

MACR···OH Complex Formation. In order to develop a master equation model of the MACR + OH addition reaction, we require a transition state structure for barrierless formation of the MACR···OH prereaction complex at 298 K. This has been achieved here by fitting a restricted (or hindered) Gorin transition state model,[34] for which all relevant properties are listed in Table 1 (using the G3SX barrier; slightly different results are obtained with the M06−2X energies, and these are tabulated in the Supporting Information). The rate constant at 298 K was set to the Lennard−Jones collision value of 5.5×10^{-10} cm^3 $molecule^{-1}$ s^{-1}. Note that this is quite similar to long-range capture rates calculated for isoprene + OH (5.54×10^{-10} cm^3 $molecule^{-1}$ s^{-1})[35] and ethene + OH (3.6×10^{-10} cm^3 $molecule^{-1}$ s^{-1}).[36] A Morse function was used to model the MACR···OH dissociation potential, which in turn was used to fit the adiabatic 2D rotor in the transition state. The equilibrium center-of-mass distance between the dissociating fragments was determined from the reduced mass and *J*-rotor of the MACR···OH complex, as described by Golden.[37] The active 1D *K*-rotor in the transition state was approximated as being equal to that of the product complex. The Gorin transition state was constructed from these 1D and 2D external rotors, all vibrations from the MACR and OH molecules (listed in the Supporting Information), and four additional degrees of freedom corresponding to internal rotational modes. The first internal rotor relates to free rotation about the axis of the dissociating MACR···OH bond, and this was assumed to be equivalent to a moment of inertia from the OH symmetric top (this assumption should be relatively robust given that OH is much smaller than MACR). The last three internal rotors constitute the "restricted" moments of inertia for the reacting fragments, made up of the remaining 1D moment from linear OH and the 2D *J*-rotor in MACR, all of which are reduced by the factor γ. This parameter is calculated as $\gamma = (1 - \eta)^{0.5}$ where η is an empirically fitted hindrance parameter which nominally varies from 0 to 1, where 0 is completely unrestricted and 1 is fully restricted.

Table 1. Parameters Used to Fit a Morse Potential and Restricted Gorin Transition State to Dissociation of the MACR···OH Complex

	Morse potential parameters
vibrational frequency of cleaving bond (cm^{-1})	162.09
dissociation energy (kcal mol^{-1})	3.1
centre of mass distance between fragments (Å)	4.01
	fitted Gorin parameters
η (−)	0.9436
γ (−)[a]	0.2374
	moments of inertia (amu $Å^2$)
adiabatic external rotor [2D][b]	478.033
active external rotor [1D]	246.057
MACR···OH internal rotor [1D]	0.897
OH fragment internal rotor; full/restricted [1D]	0.897/0.213
MACR fragment internal rotor; full/restricted [2D]	138.419/32.865

[a] $\gamma = (1 - \eta)^{0.5}$. [b] From the fitted Morse potential.

MACR + OH Addition Kinetics. Master equation simulations have been performed for OH radical addition to MACR at 298 K and 1 atm of N_2. The time-evolution of wells and products in this system is depicted in Figure 4a, whereas the evolution of vibrational energy in the major wells (**β1**, **β2**, **α1**) is depicted in Figure 4b. The activated MACR···OH complex is short-lived, essentially disappearing within a few collisions, predominantly dissociating back to the reactants. Some small fraction of the complex population passes via **TSβ1** and to a lesser extent **TSα1** to form the activated MACR−OH adducts **β1** and **α1**, which have significant excess vibrational energy but do not dissociate back to form MACR + OH to any significant extent at 298 K and 1 atm. In the case of **β1**, this excess energy is sufficient for the majority of the population to transit over **TSβ2**, yielding the *Z* isomer of the MACR−OH

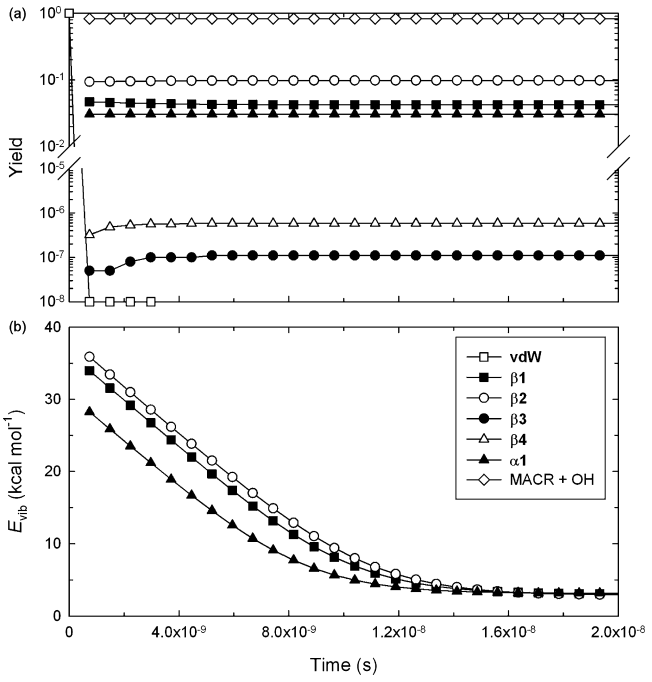

Figure 4. Results of master equation simulations of the MACR + OH reaction using G3SX barrier heights at 298 K and 1 atm N_2. (a) Well and product yields as a function of time. (b) Vibrational energy (E_{vib}) as a function of time for the important MACR−OH adducts.

DOI: 10.1021/jp303806w
J. Phys. Chem. A 2012, 116, 5317−5324

adduct, **β2**. From here, there is some minor formation of the **β3** and **β4** radicals, but not enough to be of any significance (note also that there is no formation of the enol). The final products are thus **β2** (~10%), **β1** (~4%), and **α1** (~3%), with over 80% of the initially activated complex dissociating back to MACR + OH. When the M06−2X barrier heights are used (see Supporting Information) the yields of new products are somewhat lower, due to the larger M06−2X (vs G3SX) barriers, although the reaction dynamics are similar. In both cases, the final product distribution is achieved within 4 ns. From Figure 4b, we notice that the major MACR−OH radical adducts continue to collisionally transfer energy with the bath gas until they are essentially thermalised after about 15 ns. Note that the time scale for collisional deactivation is around an order of magnitude longer than that for chemical reaction (i.e., achievement of steady-state product yields).

Calculated rate constants for β (k_2) and α (k_3) MACR + OH addition reactions are listed in Table 2, along with the total addition rate constant (k_{add}). The M06−2X results are in very good agreement with experiment, with $k_2 = 1.63 \times 10^{-11}$ cm^3 molecule^{-1} s^{-1} for the major β addition mechanism and $k_3 = 6.71 \times 10^{-13}$ cm^3 molecule^{-1} s^{-1} for the minor α addition process. On the other hand, the G3SX model results in rate constants that are too-large by around a factor of 5. A barrier height adjustment of 1.5 to 2.5 kcal mol^{-1} is required to bring the G3SX results into good agreement with experiment, which is entirely reasonable. Alternatively, the MACR + OH capture rate could be too large by around a factor of 5 (~1×10^{-10} cm^3 molecule^{-1} s^{-1}) although this seems unreasonably small. Because the reaction is essentially controlled by branching between two chemical channels, decreasing the value of ΔE_{down}, does little to increase the flux of activated [MACR···OH]* that dissociates back to MACR + OH. Considering this, and the good agreement obtained with the M06−2X model, we predominantly attribute the discrepancy between the G3SX model and experiment to the uncertainty in the calculated barrier heights.

Table 2. Theoretical Rate Constants[a] for the MACR + OH Addition Reaction from Master Equation Simulations Featuring G3SX and M06-2X Barrier Heights

	k_2	k_3	k_{add}
G3SX	7.68×10^{-11}	1.68×10^{-11}	9.35×10^{-11}
M06−2X	1.63×10^{-11}	6.71×10^{-13}	1.69×10^{-11}

[a] β addition (k_2), α addition (k_3) and total addition (k_{add}) rate constants in cm^3 molecule^{-1} s^{-1}.

Competitive O_2 Addition and Collisional Deactivation. It has been argued that, under tropospheric conditions, removal of excess vibrational energy from chemically activated [VOC−OH]* radicals by bath gas collisions (N_2, O_2) may proceed on a similar time scale to O_2 addition, allowing for the formation of doubly activated peroxyl radicals, denoted [VOC−OH−O_2]**. This process could be important if a significant fraction of the peroxyl radical population was formed with enough energy to undergo unimolecular decomposition to form new products.

Competitive O_2 addition has been incorporated into the MACR + OH master equation model developed here so as to explore the possibility of doubly activated peroxyl radical formation. To begin with, transition state structures are required for the O_2 addition transition states, which correspond to barrierless C−O_2 bond formation. These transition state structures are also essential for future modeling of unimolecular MACR−OH−O_2 reactions. Again, the restricted Gorin approach is adopted, where rate constants for the five unique O_2 addition reactions (blue pathways in Figure 1) are set to 1×10^{-11} cm^3 molecule^{-1} s^{-1}, a typical high-pressure limit value for radical − O_2 recombinations. Transition state properties are listed in Table 3. The transition states were modeled using the MACR−OH vibrational frequencies along with that of the O−O stretch in molecular oxygen (1792.46 cm^{-1}). The four unique peroxyl radicals (designated **Pα1**, **Pβ1**, **Pβ2**, **Pβ3**) were optimized at both levels of theory to obtain the external 1D *K*-rotor for the transition states and dissociation energies for fitting the Morse potentials. The center-of-mass distance between MACR−OH and O_2 in the equilibrium geometries was determined as for MACR + OH, although some of the distances needed to be decreased by around 0.2 Å in order for the Morse fit to succeed. The Morse potentials resulted in external 2D *J*-rotors for the transition states with moments on the order of 500 amu Å^2, comparable to that for the looser yet lighter MACR···OH complex formation transition state (478.033 amu Å^2, along with a slightly larger *K*-rotor). In fitting the restricted Gorin transition states, one of the

Table 3. Parameters Used to Fit a Morse Potential and Restricted Gorin Transition State to Dissociation of the MACR−OH−O_2 Adducts to MACR−OH Radicals + O_2

	α1	β1	β2	β3	β4
			Morse potential parameters		
vibrational frequency for cleaving bond (cm^{-1})	1006.29	877.77	877.77	1087.86	880.79
dissociation energy (kcal mol^{-1})	32.80	24.70	22.70	34.90	23.80
center of mass distance between fragments (Å)	3.60	3.61	3.55	3.71	3.67
			fitted Gorin parameters		
η (−)	0.9982	0.9993	0.9986	0.9988	0.9993
γ (−)[a]	0.0426	0.0260	0.0374	0.0348	0.0273
			moments of inertia (amu Å^2)		
adiabatic external rotor [2D][b]	566.994	555.831	527.915	583.389	478.033
active external rotor [1D]	187.936	193.175	193.175	192.505	173.844
MACR−OH···O_2 internal rotor [1D]	11.325	11.325	11.325	11.325	11.325
O_2 fragment internal rotor; full/restricted [1D]	11.325/0.482	11.325/0.295	11.325/0.424	11.325/0.394	11.325/0.309
MACR−OH fragment internal rotor; full/restricted [2D]	171.018/7.277	227.790/5.928	129.152/4.833	128.186/4.455	202.7571/5.538

[a] $\gamma = (1 - \eta)^{0.5}$. [b] From the fitted Morse potential. Treated as active in the MACR + OH + O_2 simulations.

DOI: 10.1021/jp303806w
J. Phys. Chem. A 2012, 116, 5317−5324

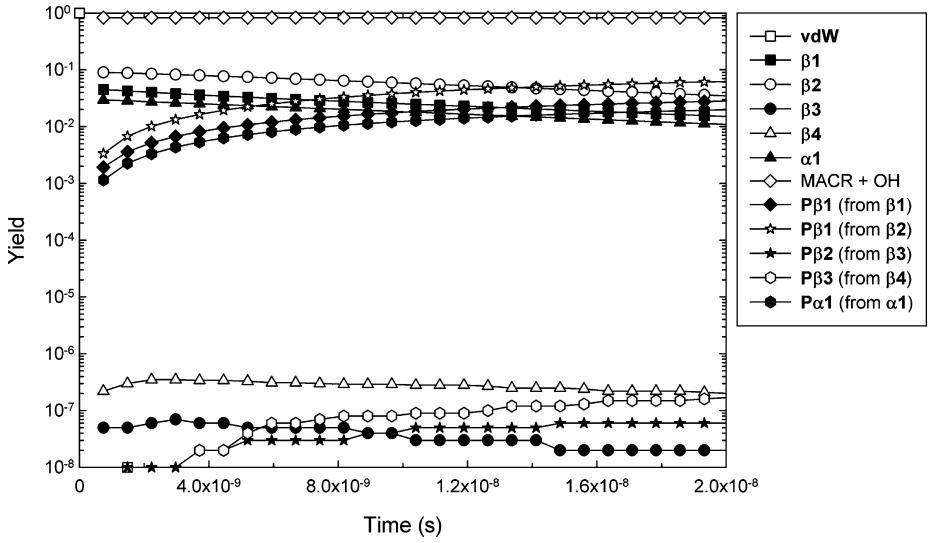

Figure 5. Well and product yields as a function of time from master equation simulations of the MACR + OH + O_2 reaction using G3SX barrier heights at 298 K and 1 atm N_2.

symmetric external rotors (11.325 amu Å^2) from the smaller O_2 fragment was assigned as being the free R···O_2 internal rotor, with the other forming the required restricted 1D rotor (with the remaining degrees of freedom satisfied by restricting the reacting MACR−OH radical 2D *J*-rotor). For the five unique transition state structures, the hindrance parameters η are 0.998 or greater, compared to 0.9436 in the MACR + OH transition state. This suggests that the reacting fragments in peroxyl radical formation access much less of the complete configuration space than for MACR + OH, consistent with tighter transition states and lower rate constants.

There has been relatively little work on incorporating secondary bimolecular reactions within a single master equation framework. Maranzana et al.[38] previously developed a single acetyl radical + O_2 + O_2 master equation using the MultiWell code, and although a somewhat different approach is adopted here much inspiration is taken from that work. We have incorporated the bimolecular MACR−OH + O_2 reactions into the MACR + OH master equation model as irreversible sinks proceeding via supermolecular transition states. Because these reactions are barrierless, the high-pressure rate constant is expected to be insensitive to temperature/energy, allowing us to use a constant pseudo first-order rate constant and therefore employ the inverse Laplace transform (ILT) approach for $k(E)$[39,40] implemented in MultiWell. First order reaction rates are set at 5.17×10^7 s^{-1}, which is the product of the O_2 concentration in tropospheric air (5.17×10^{18} molecules cm^{-3}) and the radical + O_2 rate constant (1×10^{-11} cm^3 molecule^{-1} s^{-1}). Although the restricted Gorin transition state structures were formulated in a similar way to that for MACR + OH, now all internal and external degrees of freedom in these supermolecular transition states are treated as active in the sum of states calculations (i.e., the *K*-rotor is formally active).

Yields for all wells and products calculated with the MACR + OH + O_2 master equation using G3SX barrier heights are illustrated in Figure 5 (the corresponding M06−2X figure is provided as Supporting Information). The MACR−OH radicals are rapidly produced with similar yields to those obtained with the MACR + OH master equation. These MACR−OH radicals then undergo first order decay as the MACR−OH−O_2 peroxyl radicals are being formed. This would continue until the MACR−OH radicals are completely removed. Interestingly, the subsequent formation of peroxyl radicals takes place on a longer time scale than MACR−OH formation, but one that is comparable to collisional deactivation (cf. Figure 4b). For example, at between 12 to 14 ns peroxyl radical concentrations are equivalent to those of the MACR−OH precursors, which in turn corresponds to the point at which the MACR−OH radicals effectively become quenched. As such, around 50% of the population of each peroxyl radical will be formed with some identifiable energy above that of the singly activated [MACR−OH−O_2]* adduct, and is designated as being "doubly activated" ([MACR−OH−O_2]**).

So as to further explore the additional energy imparted to these [MACR−OH−O_2]** radicals, excess vibrational energies of the important MACR−OH ***β*2** and ***β*3** radicals are plotted against the fraction of peroxyl radical formed, f_P, where f_P = [MACR−OH−O_2]/([MACR−OH−O_2]+[MACR−OH]) in Figure 6. Our results suggest that a non-negligible fraction of the MACR−OH−O_2 radical yield will be formed in a highly

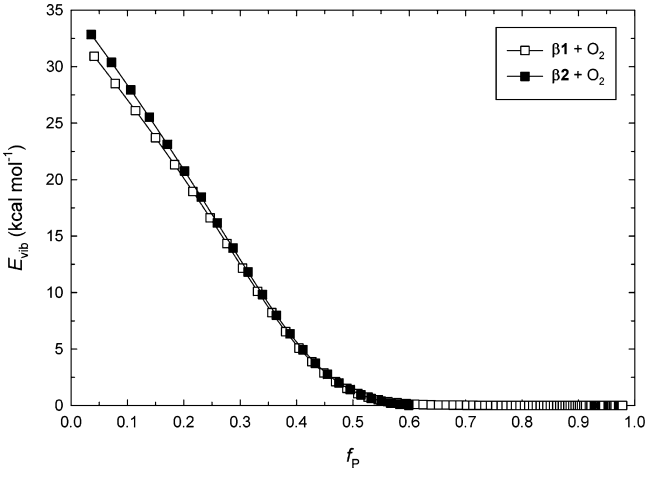

Figure 6. Excess vibrational energy (E_{vib}) of MACR−OH−O_2 peroxyl radicals as a fraction of peroxyl radical formed (f_P) from the ***β*1** and ***β*2** + O_2 reactions in MACR + OH + O_2 master equation simulations using G3SX barrier heights at 298 K and 1 atm N_2.

DOI: 10.1021/jp303806w
J. Phys. Chem. A 2012, 116, 5317−5324

Scheme 1. Unimolecular Decomposition Mechanism for the Major MACR−OH−O_2 Peroxyl Radical (Pβ1) to Form Methylglyoxal + HCHO + OH and Hydroxyacetone + CO + OH

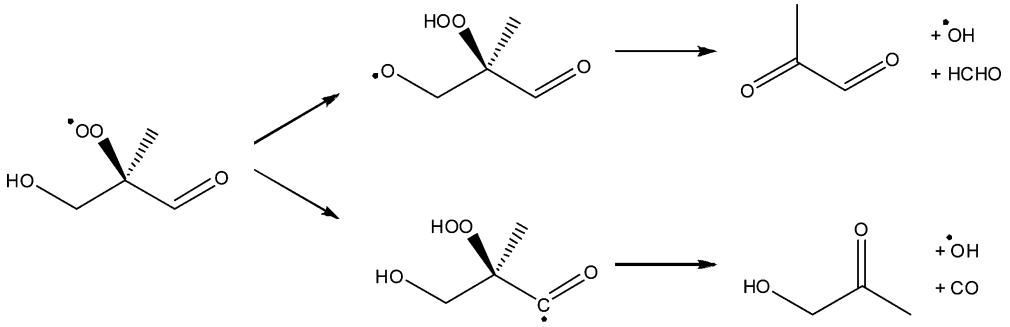

vibrationally excited state, with around 20% of the major **β2** and **β3** radicals possessing about 20 kcal mol^{-1} of vibrational energy when they react with O_2. Considering that O_2 addition releases over 20 kcal mol^{-1} in additional vibrational energy, the **Pβ1** and **Pβ2** radicals will be formed with a significant population carrying over 40 kcal mol^{-1} of vibrational energy. This should be sufficient energy to achieve some chemically activated dissociation to hydroxyacetone + CO + OH and methylglyoxal + HCHO + OH (Scheme 1) as well as reverse reaction to MACR−OH + O_2; reactions identified by Asatryan et al. as having barriers on the order of 20 kcal mol^{-1} in the analogous acrolein−OH−O_2 radicals. Hydroxyacetone and methylglyoxal are both known oxidation products of isoprene, and the potential formation of hydroxyacetone is of particular interest as atmospheric chemistry models currently underpredict its formation from isoprene photooxidation.[41]

Of course, there are uncertainties associated with the calculations presented here which will affect the excess vibrational energy carried by the MACR−OH−O_2 peroxyl radicals. The most significant uncertainty relates to the collisional energy transfer properties of MACR−OH, but even using very large values of ΔE_{down}, we find that some fraction of the MACR−OH−O_2 products carry over significant excess energy. It is clear though that experimental validation of this mechanism is now required, along with theoretical modeling of peroxyl radical decomposition as a function of internal energy. Because the double activation mechanism considered here is highly sensitive to both pressure and O_2 concentration, (O)VOC oxidation experiments observing reaction products and/or OH radical concentration as a function of both total pressure and O_2 partial pressure may be able to quantify the extent to which this mechanism operates.

CONCLUSIONS

A master equation model has been developed for the addition of OH to MACR, so as to explore competition between chemical reaction and collisional deactivation of the vibrationally excited [MACR−OH]* radicals. Furthermore, the subsequent addition of O_2 to these MACR−OH radicals has been incorporated within a single MACR + OH + O_2 master equation in order to investigate the possibility of doubly activated [MACR−OH−O_2]** peroxyl radical formation. Addition of OH to MACR predominantly occurs at the β carbon, in accordance with experiment, although this work identifies that around a third of the $HOCH_2C^{\bullet}(CH_3)CHO$ radical product is quenched as the higher-energy *E* isomer. Using M06−2X barrier heights, we obtain purely theoretical rate constants that are in good agreement with experiment, whereas using G3SX barriers, the known rate constants are overpredicted. We find that collisional deactivation of MACR−OH radical adducts takes place on a significantly longer time scale than chemical reaction. When secondary O_2 addition is incorporated into the reaction model this results in significant formation of doubly activated peroxyl radicals; for example, 20% of the major $HOCH_2C^{\bullet}(CH_3)CHO$ radical population possesses over 20 kcal mol^{-1} in vibrational energy when it reacts with O_2. The formation of doubly chemically activated peroxyl radicals opens up the possibility of prompt unimolecular decomposition and hydroxyl radical regeneration from OH addition to unsaturated VOCs and OVOCs in the troposphere.

ASSOCIATED CONTENT

Supporting Information

Optimized geometries, vibrational frequencies, and moments of inertia for reactants and wells. Properties for restricted Gorin transition states obtained using M06−2X barrier heights. Results of master equation simulations with M06−2X barrier heights. This material is available free of charge via the Internet at http://pubs.acs.org.

AUTHOR INFORMATION

Corresponding Author

*E-mail: gdasilva@unimelb.edu.au.

Notes

The authors declare no competing financial interest.

ACKNOWLEDGMENTS

This work was supported by the Australian Research Council (ARC) through the Discovery Projects scheme (DP110103889). Computational resources provided in part by the Victorian Partnership for Advanced Computing (VPAC).

REFERENCES

(1) Tan, D.; Faloona, I.; Simpas, J. B.; Brune, W.; Shepson, P. B.; Couch, T. L.; Sumner, A. L.; Carroll, M. A.; Thornberry, T.; Apel, E.; Riemer, D.; Stockwell, W. *J. Geophys. Res.* **2001**, *D20*, 24407−24427.

(2) Carslaw, N.; Creasey, D. J.; Harrison, D.; Heard, D. E.; Hunter, M. C.; Jacobs, P. J.; Jenkin, M. E.; Lee, J. D.; Lewis, A. C.; Pilling, M. J.; Saunders, S. M.; Seakins, P. W. *Atmos. EnViron.* **2001**, *35*, 4725−4737.

(3) Thornton, J. A.; Woolridge, P. J.; Cohen, R. C.; Martinez, M.; Harder, H.; Brune, W. H.; Williams, E. J.; Roberts, J. M.; Fehsenfeld, F. C.; Hall, S. R.; Shetter, R. E.; Wert, B. P.; Fried, A. *J. Geophys. Res.* 2002, *107*, doi: 10.1029/2001JD000932.

DOI: 10.1021/jp303806w
J. Phys. Chem. A 2012, 116, 5317−5324

(4) Lelieveld, J.; Butler, T. M.; Crowley, J. N.; Dillon, T. J.; Fischer, H.; Ganzeveld, L.; Harder, H.; Lawrence, M. G.; Martinez, M.; Taraborrelli, D.; Williams, J. *Nature* **2008**, *452*, 737.
(5) Di Carlo, P.; Brune, W. H.; Martinez, M.; Harder, H.; Lesher, R.; Ren, X.; Thornberry, T.; Carroll, M. A.; Young, V.; Shepson, P. B.; Riemer, D.; Apel, E.; Campbell, C. *Science* **2004**, *304*, 722.
(6) Hofzumahaus, A.; Rohrer, F.; Lu, K.; Bohn, B.; Brauers, T.; Chang, C.-C.; Fuchs, H.; Holland, F.; Kita, K.; Kondo, Y.; Li, X.; Lou, S.; Shao, M.; Zeng, L.; Wahner, A.; Zhang, Y. *Science* **2009**, *324*, 1702.
(7) Montzka, S. A.; Trainer, M.; Goldan, D.; Kuster, W. C.; Fehsenfeld, F. C. *J. Geophys. Res.* **1993**, *98*, 1101.
(8) Warneke, C.; Holzinger, R.; Hansel, A.; Jordan, A.; Lindinger, W.; Pöschl, U.; Williams, J.; Hoor, P.; Fischer, H.; Crutzen, P. J.; Scheeren, H. A.; Lelieveld, J. *J. Atmos. Chem.* **2001**, *38*, 167.
(9) Pierotti, D.; Wofsy, S. C.; Jacob, D.; Rasmussen, R. A. *J. Geophys. Res.* **2004**, *95*, 1871.
(10) Gierczak, T.; Burkholder, J. B.; Talukdar, R. K.; Mellouki, A.; Barone, S. B.; Ravishankara, A. R. *J. Photochem. Photobiol. A: Chem.* **1997**, *110*, 1.
(11) Tuazon, E. C.; Atkinson, R. *Int. J. Chem. Kinet.* **1990**, *22*, 591.
(12) Orlando, J. J.; Tyndall, G. S. *Geophys. Res. Lett.* **1999**, *26*, 2191.
(13) Chuong, B.; Stevens, P. S. *J. Phys. Chem. A* **2003**, *107*, 2185.
(14) Ochando-Pardo, M.; Nebot-Gil, I.; Gonzalez-Lafont, A. *ChemPhysChem* **2005**, *6*, 1567.
(15) Vega-Rodriguez, A.; Alvarez-Idaboy, J. R. *Phys. Chem. Chem. Phys.* **2009**, *11*, 7649.
(16) Asatryan, R.; da Silva, G.; Bozzelli, J. W. *J. Phys. Chem. A* **2010**, *114*, 8302.
(17) da Silva, G.; Graham, C.; Wang, Z.-F. *Environ. Sci. Technol.* **2010**, *44*, 250.
(18) Peeters, J.; Nguyen, T. L.; Vereecken, L. *Phys. Chem. Chem. Phys.* **2009**, *11*, 5935.
(19) da Silva, G. *J. Phys. Chem. A* **2010**, *114*, 6861.
(20) da Silva, G. *Phys. Chem. Chem. Phys.* **2010**, *12*, 6698.
(21) da Silva, G. *J. Phys. Chem. A* **2011**, *115*, 291.
(22) Crounse, J. D.; Knap, H. C.; Ornso, K. B.; Jorgensen, S.; Paulot, F.; Kjaergaard, H. G.; Wennberg, P. O. *J. Phys. Chem. A* **2012**, DOI: 10.1021/jp211560u.
(23) Curtiss, L. A.; Redfern, P. C.; Raghavachari, K.; Pople, J. A. *J. Chem. Phys.* **2001**, *114*, 108.
(24) Zhao, Y.; Truhlar, D. G. *Theor. Chem. Acc.* **2008**, *120*, 215.
(25) Zheng, J.; Zhao, Y.; Truhlar, D. G. *J. Chem. Theory Comput.* **2009**, *5*, 808.
(26) Frisch, M. J.; Trucks, G. W.; Schlegel, H. B.; Scuseria, G. E.; Robb, M. A.; Cheeseman, J. R.; Scalmani, G.; Barone, V.; Mennucci, B.; Petersson, G. A. et al.. *Gaussian 09, Revision B.01*; Gaussian, Inc., Wallingford CT, 2010.
(27) Ortiz, N. F.; Preses, J. M.; Lohr, L. L.; Maranzana, A.; Stimac, P. J.; Nguyen, T. L.; Kumar, T. J. D. *MultiWell-2011.3 Software*, 2011, designed and maintained by John R. Barker with contributors; University of Michigan: Ann Arbor, MI; http://aoss.engin.umich.edu/multiwell/.
(28) Barker, J. R. *Int. J. Chem. Kinet.* **2001**, *33*, 232.
(29) Barker, J. R. *Int. J. Chem. Kinet.* **2009**, *41*, 748.
(30) Nguyen, T. L.; Barker, J. R. *J. Phys. Chem. A* **2010**, *114*, 3718.
(31) Archibald, A. T.; McGillen, M. R.; Taatjes, C. A.; Percival, C. J.; Shallcross, D. E. *Geophys. Res. Lett.* **2007**, *34*, L21801.
(32) Paulot, F.; Crounse, J. D.; Kjaergaard, H. G.; Kroll, J. H.; Seinfeld, J. H.; Wennberg, P. O. *Atmos. Chem. Phys.* **2009**, *9*, 1479.
(33) da Silva, G. *Angew. Chem., Int. Ed.* **2010**, *49*, 7523.
(34) Smith, G. P.; Golden, D. M. *Int. J. Chem. Kinet.* **1978**, *10*, 489.
(35) Greenwald, E. E.; North, S. W.; Georgievskii, Y.; Klippenstein, S. J. *J. Phys. Chem. A* **2007**, *111*, 5582.
(36) Greenwald, E. E.; North, S. W.; Georgievskii, Y.; Klippenstein, S. J. *J. Phys. Chem. A* **2005**, *109*, 6031.
(37) Golden, D. M. *Int. J. Chem. Kinet.* **2009**, *41*, 573.
(38) Maranzana, A.; Barker, J. R.; Tonachini, G. *Phys. Chem. Chem. Phys.* **2007**, *9*, 4129.
(39) Forst, W. *J. Phys. Chem.* **1972**, *76*, 342.
(40) Forst, W. *J. Phys. Chem.* **1982**, *86*, 1771.
(41) Karl, T.; Guenther, A.; Turnipseed, A.; Tyndall, G.; Artaxo, P.; Martin, S. *Atmos. Chem. Phys.* **2009**, *9*, 7753.

DOI: 10.1021/jp303806w
J. Phys. Chem. A 2012, 116, 5317−5324